Tunable Transmission Resonant Filter and Modulator With Vertical Gratings

Hyo-Chang Kim, Kazuhiro Ikeda, and Yeshaiahu Fainman, *Fellow, IEEE*

***Abstract*—Resonant filters in waveguides with vertical gratings have been realized on a silicon-on-insulator wafer. Two identical uniformly distributed Bragg reflectors with vertical gratings are separated by a quarter wavelength phase offset. Experimental studies show a broad stopband and a narrow transmission band which shifts with changing substrate temperature that is also illuminated by an external laser pump beam at 514-nm wavelength. Experimental results on a low-frequency thermal modulation using an external light source are also presented.**

***Index Terms*—Distributed Bragg reflector (DBR), optical filters, silicon-on-insulator (SOI) technology, thermooptic effects.**

I. Introduction

SPATIALLY corrugated reflectors, which are employed in distributed feedback lasers in active waveguides and in distributed Bragg reflectors (DBR) in passive waveguides, have been used in various optical devices, including single-mode semiconductor lasers, passive optical filters, modulators, beam couplers, and sensors [1]–[5]. Passive optical filters made up of a periodic structure possess a stopband in their transmission spectra. Moreover, when a pair of such periodic structures is separated by a quarter wavelength phase offset, a narrow resonant transmission mode appears in the center of the stopband [2], [4], [5]. Advances in device fabrication technology enabled the definition of periodic structures on sidewalls of a high mesa waveguide first developed for a single-mode operation of high index contrast laser devices on InP [6]–[8]. In this paper, we apply a vertical grating approach to implement a resonant filter and a resonant modulator using a silicon-on-insulator (SOI) material system.

II. Theory

We exploit a resonant transmission filter consisting of a pair of periodic structures separated by a quarter wavelength phase offset. The top view of the device is shown schematically in Fig. 1(a). Here, W_S is the average width of the waveguide,

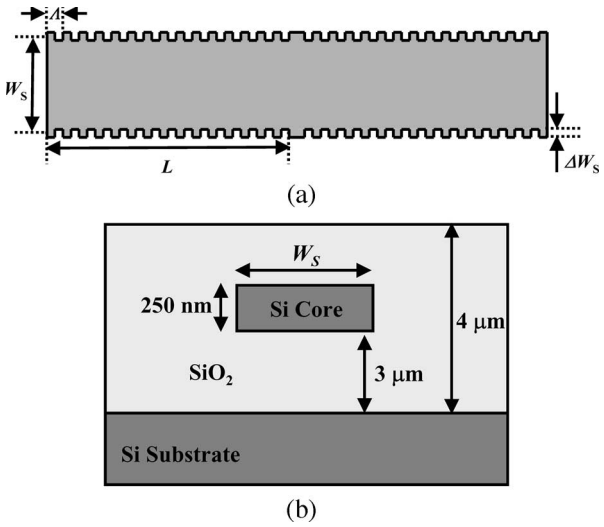

Fig. 1. (a) Schematic diagram of the top view of quarter wavelength shifted transmission resonant filter with vertical gratings, where W_S is the average width of the waveguide, ΔW_S is the full depth of a single side of the vertical grating, and L and Λ are the total length and the period of a single Bragg reflector, respectively. (b) Cross section of the transmission resonant filter.

ΔW_S is the full depth of single side of the vertical grating, and L and Λ are the length and the period of a single Bragg reflector, respectively. The separation between the two Bragg reflectors is set to a quarter wavelength phase offset that is also equal to a half period $(\Lambda/2)$ of the Bragg reflectors. The latter creates a longitudinal single mode cavity to introduce a narrow transmission band in the wide stopband of the Bragg reflector. The coupling coefficient (κ) of a fundamental lateral-mode first-order Bragg reflector for transverse electric (TE) field, where electric field is parallel to the wafer surface, is given by [3]

$$\kappa = \Gamma \left[\frac{\pi}{\lambda}\frac{\Delta W_S}{W_{\text{eff}}}\frac{n_S^2 - n^2}{nq}\right]\left[\frac{n^2}{n_S^2} - \frac{n^2}{n_{\text{SiO2}}^2} + 1\right] \quad (1)$$

where $q \equiv (n/n_S)^2 + (n/n_{\text{SiO2}})^2 - 1$, $W_{\text{eff}} \equiv W_S + 2/(q\gamma)$, $\gamma \equiv (\beta^2 - k^2 n_{\text{SiO2}}^2)^{1/2}$, and $n \equiv \beta/k$. Here, Γ is a power fraction confined in the silicon core for TE polarization (∼85%) [9]. β, $k(= 2\pi/\lambda)$, and λ are the propagation constant, wavenumber, and wavelength in a vacuum, respectively. A cross section of the device is shown in Fig. 1(b). n_S is the effective index of a three layer slab waveguide consisting of a silicon core layer and two silicon dioxide cladding layers, calculated using Newton's method [10]. Here, the refractive indexes of silicon and silicon dioxide n_{SiO2} are assumed to be 3.5 and

Manuscript received April 5, 2006; revised February 2, 2007. This work was supported in part by the National Science Foundation, by the Air Force Office of Scientific Research, and by the Defense Advanced Research Projects Agency. The work of K. Ikeda was supported by a scholarship from Nakajima Foundation, Japan.

The authors are with the Department of Electrical and Computer Engineering, University of California at San Diego, La Jolla, CA 92093-0407 USA (e-mail: hckim@emerald.ucsd.edu; kazikeda@ucsd.edu; fainman@ece.ucsd.edu).

Color versions of one or more of the figures in this paper are available online at http://ieeexplore.ieee.org.

Digital Object Identifier 10.1109/JLT.2007.893922

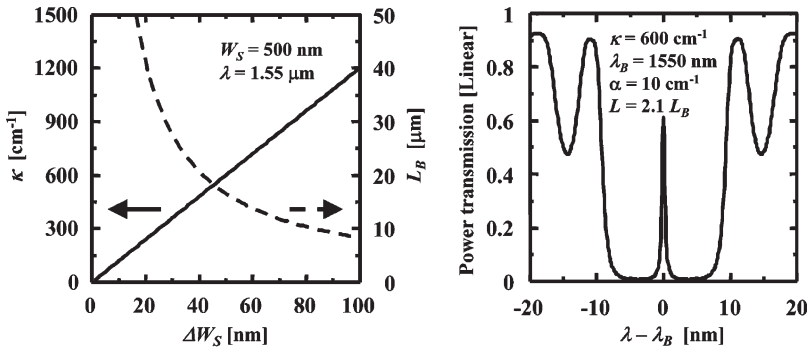

Fig. 2. (a) Calculated coupling coefficient (κ) and corresponding Bragg length $(L_B = 1/\kappa)$ versus ΔW_S. (b) Simulated transmission power versus $(\lambda - \lambda_B)$.

1.4, respectively. Fig. 2(a) shows the calculated κ and its inverse corresponding to the Bragg length $(L_B = 1/\kappa)$ with $W_S = 500$ nm and $\lambda = 1550$ nm. The value of $\Delta W_S = 50$ nm yields $\kappa \sim 600$ cm^{-1} and the corresponding $L_B \sim 16.6$ μm. Next, we calculate the transmission amplitude of the resonant filter $(t_{\rm RF})$ as a function of the wavelength (λ), assuming Bragg reflectors with field reflectivity (r) and transmission (t), and a phase shift (ϕ) introduced by the length of the spacer (d) between the two Bragg reflectors by

$$t_{\rm RF} = \frac{t^2 \exp(i\phi)}{1 - r^2 \exp(2i\phi)} \tag{2}$$

where $t = 1/(\cosh(\mu L) - (i\delta - \alpha/2)\sinh(\mu L)/\mu)$, $r = -i\kappa \sinh(\mu L)t/\mu$, $\mu^2 \equiv \kappa^2 + (i\delta - \alpha/2)^2$ with detuning parameter $\delta \equiv \beta - \beta_B \sim (d\beta/d\omega)(\omega - \omega_B) = (\omega - \omega_B)/\nu_g$, α is the loss of Bragg reflector, ω is the angular frequency, $\omega_B (\equiv 2\pi c/\lambda_B)$ is the Bragg angular frequency, $\nu_g (\equiv c/n_g)$ is the group velocity of the waveguide, c is the speed of light in a vacuum, $\lambda_B (= 2n\Lambda)$ is the Bragg wavelength, and $n_g (= n - \lambda_B(\Delta n/\Delta\lambda) = 3.8)$ is the group index of the waveguide [2], [5]. In (2), we assume that κ is a constant over the wavelength of interest [2], which can be confirmed by (1) and enables efficient calculation. $|t_{\rm RF}|^2$ is periodic in ϕ with period π, supporting the transmission resonances occurring in the center of the stopband in odd multiples of $\pi/2$. However, this resonance can be tuned by varying the length of the spacer (d). Fig. 2(b) shows a plot of $|t_{\rm RF}|^2$, assuming values of $\kappa = 600$ cm^{-1}, $\alpha = 10$ cm^{-1}, $\lambda_B = 1550$ nm, $d = \lambda_B/(4n)$, $\phi = \beta_B \times d = \pi/2$, $L = 2.1 \times L_B$, and $n_g = 3.8$.

III. Fabrication

The designed devices are fabricated on a small piece $(\sim 0.5$ cm$^2)$ taken from a 15.24-cm SOI wafer consisting of a silicon top layer with a mean thickness of 252.2 nm, with a distribution of $6\sigma \sim 18.3$ nm on a ~ 3-μm-thick silicon dioxide layer which, in turn, is on a $\langle 100 \rangle$ p-type silicon substrate with a resistivity of 14–22 $\Omega \cdot$ cm. A scanning electron microscope (SEM) with a pattern generation software is used to pattern the whole structure on an area of $\sim 150 \times 300$ μm^2. Following a standard liftoff process to transfer the pattern to a nickel mask, the silicon layer is selectively etched in a reactive ion etcher using a mixture of BCl_3/Ar with gas flow rates of $BCl_3/Ar = 10/10$ sccm, pressure of $\sim$30 mtorr, power density of ~ 0.1 W/cm^2, and temperature of ~ 20 °C. It results in an etching rate of $\sim$75 nm/min for a sample size of ~ 0.5 cm^2. Fig. 3(a) and (b) shows the top and tilted SEM images of the etched structures, respectively. After removing the nickel, a buffer layer of silicon dioxide that is $\sim$1-μm thick is sputtered to obtain a symmetry in the vertical direction, and the silicon substrate is polished down to ~ 50 μm to facilitate the cleaving. In addition, a single-step antireflection coating (Si_3N_4) was sputtered on the cleaved facets of the device to reduce the Fabry–Pérot (FP) resonance at the air-silicon interfaces. Samples were suspended on a carbon tape using a glass plate for fiber couplings.

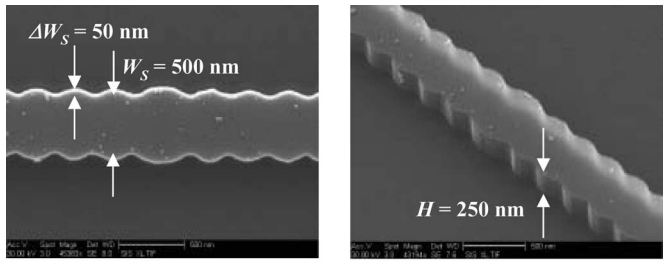

Fig. 3. Scanning electron micrographs of a dry etched device sample. (a) Top view. (b) Tilted view.

IV. Results and Discussion

A broadband source centered at 1.56 μm is coupled into a fiber-optic polarizer, followed by a polarization maintaining (PM) tapered fiber with an output spot diameter of ~ 2.5 μm, producing $\sim$20-dB polarization extinction. A pair of such PM tapered fibers is used to couple light into and out of the fabricated devices. We used a 2-μm-wide waveguide on the chip for fiber coupling, in which case, $\sim 1\%$ power from the input PM fiber is delivered to the output PM fiber. The measurements are performed using TE-polarized input light and optical spectrum analyzer. After measuring both transmission spectra from the device and broadband source with the same resolution and wavelength range, each data measured from the device is

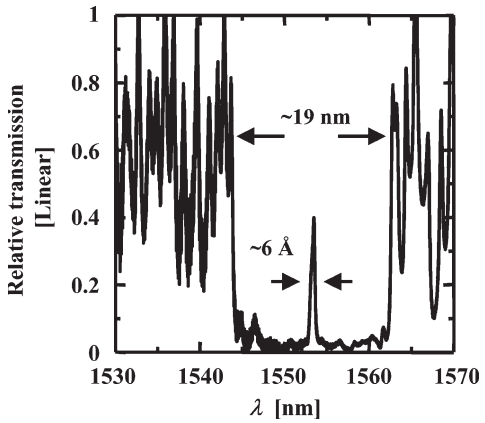

Fig. 4. Measured transmission spectrum of the device at TE polarization.

divided by the one from the broadband source. Fig. 4 shows a typical measured device spectrum. Oscillatory behavior outside of the stopband and a slight asymmetry of the resonant transmission band are most likely due to residual reflections on the two Si_3N_4 coated facets. The measured spectrum shown in Fig. 4 is in good agreement with the calculated prediction in Fig. 2(b). Next, we investigate the thermal tuning of the resonant transmittance by mounting the fabricated device on a thermoelectric cooler. Fig. 5(a) shows that resonant transmittance shifts by ~4 nm when the temperature is increased by 50 K. Although the temperature dependence of the refractive index of silicon dioxide is one order of magnitude weaker than the refractive index for silicon and ~20% of the guided mode power is present in silicon dioxide, calculations reveal that the effective index change (Δn) is nearly proportional to the index change of the silicon core at a fixed wavelength for the wavelength range of interest. Provided that the resonant transmittance band wavelength mainly depends on the index change $\Delta\lambda_B/\Delta T \sim 2(\Delta n/\Delta T)\Lambda \sim 2(\Delta n_{\rm Si}/\Delta T)\Lambda$, where Δn and $\Delta n_{\rm Si}$ are the effective index changes of the guided mode and the silicon core as a function of T, and $\Lambda = 305$ nm, $\Delta n_{\rm Si}/\Delta T$ is estimated to be $\sim 1.3 \times 10^{-4}$ K^{-1}. This value is smaller than those reported by other research groups [11], [12]. For example, Li searched, compiled, and analyzed various measured refractive index data for silicon and recommended its temperature derivative value of $\Delta n_{\rm Si}/\Delta T \sim (1.8 \pm 0.15) \times 10^{-4}$ K^{-1} at $\lambda = 1550$ nm and $T = 293$ K [11]. Della Corte *et al.* measured and modeled $\Delta n_{\rm Si}/\Delta T \sim 1.76 \times 10^{-4}$ K^{-1} at $\lambda = 1550$ nm and $T = 300$ K with an error of 6.5% [12]. However, material dispersion of the silicon core and structural dispersion over the tuning spectral range should be additionally considered in this paper. The latter is one order of magnitude larger than the former, while both effects decrease the effective index and are included in the equation $\Delta\lambda_B/\Delta T \sim 2(\Delta n/\Delta T + (\Delta n/\Delta\lambda) \times (\Delta\lambda_B/\Delta T))\Lambda + 2n(\Delta\Lambda/\Delta T) \sim 2(\Delta n_{\rm Si}/\Delta T + (\Delta n/\Delta\lambda_B) \times (\Delta\lambda_B/\Delta T))\Lambda + 2n(\Delta\Lambda/\Delta T) \sim (\Delta n_{\rm Si}/\Delta T)\lambda_B/n_g + 2n^2(\Delta\Lambda/\Delta T)/n_g$, where all derivatives of n are evaluated at $\lambda = \lambda_B$ and $T = 20\,^{\circ}$C. The last term explains the linear thermal expansion of the period and is estimated to $\Delta\Lambda(T)/\Delta T \sim 0.8 \times 10^{-3}$ nm/K [13]. $\Delta n_{\rm Si}/\Delta T$ is interpreted as real refractive index increment of the silicon core over temperature and corresponds to $\Delta n_{\rm Si}/\Delta T \sim (0.08 - 0.0027) \times (3.8/1550) \sim 1.9 \times 10^{-4}$ K^{-1} with a value of $n_g = 3.8$. This value of $\Delta n_{\rm Si}/\Delta T$ can be compared with the previously reported values, and the contribution of thermal expansion of Λ to $\Delta\lambda_B$ is estimated to ~5%. Here, we determined the value of $n_g = 3.8 \pm 0.1$ by measuring the FP resonant mode spacing of a straight waveguide with $W_S = 500$ nm at $\lambda = 1550$ nm.

Next, we focused a continuous wave (CW) Ar-laser at a wavelength of 514 nm onto the center region of the device using a microscope objective with NA = 0.4, producing a minimum spot size of ~1.6 μm. The distance from the device to the beam waist was adjusted to assure illumination of the center of the device. Fig. 5(b) shows the shift of the resonant transmission versus the CW power of the pump. Lateral chip dimension used to measure the spectra in Fig. 5(b) is 400×700 μm^2, and the thickness of the chip is ~50 μm. The pump power of 10 mW measured at the output of the microscope objective causes a shift in the resonant transmission wavelength of ~2 nm. It should be noted that the silicon core overcoated by the silicon dioxide layer is resting on an optically and thermally isolating 3-μm-thick silicon dioxide cladding layer over the entire silicon substrate. The pump power is absorbed in the silicon layer, generating heat and changing the refractive index of the silicon. The heat generated in the silicon core should be dissipated into the silicon substrate which has larger thermal capacity. Although an absolute power absorbed in the device is not well defined experimentally, the direction of the whole spectrum movement in Fig. 5(b) indicates that the thermal distribution across the device may depend on the heat sinking method of the chip more strongly. If the size of the chip is bigger or the chip is bonded on heat sink, the heat generated by the incident power level in Fig. 5(b) will be more strongly distributed around the illuminated region and may also need more power to achieve the same movement of the resonant wavelength.

Finally, with the same sample used to measure the condition in Fig. 5(b), experiments using a square wave modulated CW Ar pump beam are conducted. We use an acousto-optic modulator driven by the square wave modulating signals at 10 kHz with measured rise and fall times of ~25 ns [see Fig. 6(a)]. The measured average modulated argon laser power at the output of the microscope objective is 1.5 mW. A tunable laser source is adjusted to the resonant transmission of the device at $\lambda \sim 1554.8$ nm. When the modulated pump beam is turned on, the output transmittance of the device is modulated, producing a modulated output signal, as shown in Fig. 6(b). An additional modulated response is found by tuning the input signal wavelength to ~1555.5 nm. It should be noted that the spot sizes in Figs. 5(b) and 6(b) are not the same. The measured values of 10 μs or less for the rise time and fall time [see Fig. 6(b)] are comparable with the values found in various devices fabricated on SOI wafers [14]–[17].

V. Conclusion

Transmission resonant filters with vertical gratings have been realized on the SOI wafer. The resonant filter is constructed in a 500-nm-wide waveguide using a pair of 35-μm-long (2.1 times Bragg length) DBRs, each implemented using vertical gratings

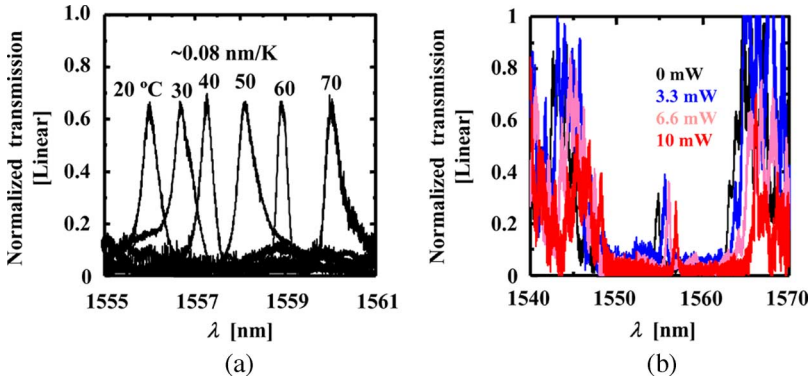

Fig. 5. (a) Transmission spectra of the resonant mode for substrate temperature varying in the range of 20 °C–70 °C. (b) Transmission spectra of the resonant mode for irradiance of the cavity region of the device by the CW argon laser at power levels varying in the range of 0–10 mW.

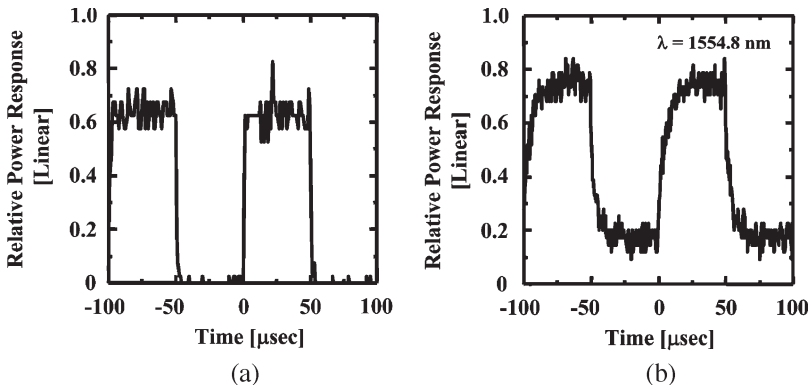

Fig. 6. (a) Power versus time trace of the modulated argon laser beam used to pump the cavity region of the device. (b) Output power versus time of the device operating at a wavelength of $\lambda = 1554.8$ nm, when the cavity region of the device is modulated by the modulated argon laser with an average power of about 1.5 mW.

with 50-nm depth. These two resonant Bragg reflectors are separated by a 152-nm-long spacer, realizing a half period of the Bragg grating and introducing a narrow transmittance band in the center of the wide stopband of the Bragg reflectors. The measured linewidth of the resonant transmittance band and the bandwidth of the stopband are ∼0.6 and ∼19 nm, respectively. Substrate temperature tuning of the resonant transmission band of ∼0.08 nm/K is found experimentally. A pump laser with a photon energy larger than the bandgap for silicon is also used to transfer a thermal energy to the device showing experimentally measured transmittance band tuning versus optical pump power coefficient of ∼0.2 nm/mW. Finally, by using this thermal effect of refractive index change, we succeed in operating the device as a modulator at 1.55 μm using an optical pump at 514 nm modulated at 10 kHz with ∼3-mW incident power.

ACKNOWLEDGMENT

The authors would like to thank R. Saperstein, M. Nezhad, K. Tetz, and U. Levy for their help with the experimental setup, B. R. Henry at Trion Technology for suggesting their silicon etching with $BCl_3/Cl_2/Ar$ mixtures, A. Krishnamoorthy and J. Cunningham at Sun Microsystems for the valuable suggestions and encouragement, and D. Aplin for the english corrections. The authors would also like to thank the anonymous reviewers for many valuable and fruitful comments.

REFERENCES

[1] H. Kogelnik, "Theory of dielectric waveguides," in *Topics in Applied Physics 7, Integrated Optics*, T. Tamir, Ed. New York: Springer-Verlag, 1979, pp. 13–81.
[2] H. A. Haus, *Waves and Fields in Optoelectronics*. Englewood Cliffs, NJ: Prentice-Hall, 1984, pp. 235–253.
[3] D. G. Hall, "Optical waveguide diffraction gratings: Coupling between guided modes," in *Progress in Optics*, vol. XXIX, E. Wolf, Ed. Amsterdam, The Netherlands: North-Holland, 1991, pp. 1–63.
[4] Y. Suematsu and A. R. Adams, *Handbook of Semiconductor Lasers and Photonic Integrated Circuits*. New York: Chapman & Hall, 1994.
[5] C. H. Henry, Y. Shani, R. C. Kisler, T. E. Jewell, V. Pol, N. A. Olsson, R. F. Kazarinov, and K. J. Orlowski, "Compound Bragg reflection filters made by spatial frequency doubling lithography," *J. Lightw. Technol.*, vol. 7, no. 10, pp. 1379–1385, Oct. 1989.
[6] J. Wiedmann, K. Ebihara, H. C. Kim, B. Chen, M. Ohta, K. Matsui, S. Tamura, J.-I. Shim, and S. Arai, "1.5 μm wavelength distributed reflector lasers with vertical grating," *Electron. Lett.*, vol. 37, no. 13, pp. 831–832, Jun. 2001.
[7] H. C. Kim, J. Wiedmann, K. Matsui, S. Tamura, and S. Arai, "1.5-μm-wavelength distributed feedback lasers with deeply etched first-order vertical grating," *Jpn. J. Appl. Phys.*, vol. 40, no. 10B, pp. L1107–L1109, Oct. 2001.
[8] H. C. Kim, H. Kanjo, T. Hasegawa, S. Tamura, and S. Arai, "1.5 μm wavelength narrow stripe distributed reflector lasers for high performance operation," *IEEE J. Sel. Topics Quantum Electron.*, vol. 9, no. 5, pp. 1146–1152, Sep./Oct. 2003.
[9] G. P. Agrawal and N. K. Dutta, "Analysis of ridge-waveguide distributed feedback lasers," *IEEE J. Quantum Electron.*, vol. QE-21, no. 6, pp. 534–538, Jun. 1985.
[10] G. B. Arfken, *Mathematical Methods for Physicists*, 3rd ed. Orlando, FL: Academic, 1985, p. 963.
[11] H. H. Li, "Refractive index of silicon and germanium and its wavelength and temperature derivatives," *J. Phys. Chem. Ref. Data*, vol. 9, no. 3, pp. 561–658, Jul. 1980.

[12] F. G. Della Corte, M. E. Montefusco, L. Moretti, I. Rendina, and G. Cocorullo, "Temperature dependence analysis of the thermo-optic effect in silicon by single and double oscillator models," *J. Appl. Phys.*, vol. 88, no. 12, pp. 7115–7119, Dec. 2000.
[13] *CRC Handbook of Chemistry and Physics*, CRC, Boca Raton, FL, 2005–2006, pp. 12–77.
[14] G. V. Treyz, "Silicon Mach-Zehnder waveguide interferometers operating at 1.3 μm," *Electron. Lett.*, vol. 27, no. 2, pp. 118–120, Jan. 1991.
[15] U. Fischer, T. Zinke, B. Schüppert, and K. Petermann, "Singlemode optical switches based on SOI waveguides with large cross-section," *Electron. Lett.*, vol. 30, no. 5, pp. 406–408, Mar. 1994.
[16] R. L. Espinola, M. C. Tsai, J. T. Yardley, and R. M. Osgood, "Fast and low-power thermooptic switch on thin silicon-on-insulator," *IEEE Photon. Technol. Lett.*, vol. 15, no. 10, pp. 1366–1368, Oct. 2003.
[17] T. Asano, W. Kunishi, M. Nakamura, B. S. Song, and S. Noda, "Dynamic wavelength tuning of channel-drop device in two-dimensional photonic crystal slab," *Electron. Lett.*, vol. 41, no. 1, pp. 37–38, Jan. 2005.

Hyo-Chang Kim was born in Seoul, Korea, in 1973. He received the B.S. and M.S. degrees in electronic engineering from SungKyunKwan University, Suwon, Korea, in 1995 and 1999, respectively. In his master thesis, he studied nonparaxial properties of laser beams. He received the Ph.D. degree from the Department of Electrical and Electronic Engineering, Tokyo Institute of Technology, Tokyo, Japan in 2004. In his doctoral thesis, he studied 1.5-μm wavelength single-mode semiconductor lasers with high index contrast lateral guidance.

Since 2004, he has been a Postdoctoral Researcher with the Department of Electrical and Computer Engineering, University of California at San Diego, La Jolla, where he studies 1.5-μm wavelength passive transmission resonant filters, switches, and modulators with both high index contrast lateral and vertical guidance using silicon-on-insulator wafers.

Kazuhiro Ikeda received the B.E. and M.E. degrees in precision science from Osaka University, Suita, Japan, in 1998 and 2000, respectively. He is currently working toward the Ph.D. degree at the Department of Electrical and Computer Engineering, University of California at San Diego, La Jolla.

In 2000, he joined the Fitel Photonics Laboratory, Furukawa Electric Co., Ltd., where he worked on polarization controllers and first- and second-order polarization mode dispersion compensators. He received graduate scholarships from the Japan Student Services Organization (1998–2000) and the Nakajima Foundation (since 2004). His research interests include nanoscale optical devices and nonlinear processes in optical resonators.

Yeshaiahu Fainman (M'93–SM'01–F'03) received the Ph.D. degree from Technion, Israel Institute of Technology, Haifa, Israel, in 1983.

He is a Professor of electrical and computer engineering with the University of California at San Diego, La Jolla. His current research interests are in near-field phenomena in optical nanostructures and nanophotonic devices, nonlinear space-time processes using femtosecond laser pulses for optical communications, quantum cryptography and communication, diffractive and nonlinear optics, and multidimensional quantitative imaging. He has contributed over 160 manuscripts in referred journals and over 280 conference presentations and conference proceedings.

Dr. Fainman is a Fellow of the Optical Society of America, and the Society of Photo-Optical Instrumentation Engineers and is a recipient of the Miriam and Aharon Gutvirt Prize. He has been a Chair of IEEE/LEOS sub-Committee on Optical Interconnects and Signal Processing since 2004 and was a General Chair for the Inaugural OSA Topical Meeting on Nanophotonics for Information Systems in 2005. He also served on numerous conference program committees, organized symposium and workshops, and between 1993 and 2001, he served as a Topical Editor of the *Journal of the Optical Society of America: A* on Optical Signal Processing and Imaging Science.